ISSN 0021-3640, JETP Letters, 2019, Vol. 109, No. 9, pp. 594–599. © Pleiades Publishing, Inc., 2019.
Russian Text © The Author(s), 2019, published in Pis'ma v Zhurnal Eksperimental'noi i Teoreticheskoi Fiziki, 2019, Vol. 109, No. 9, pp. 615–620.

CONDENSED MATTER

Kinetics of the Atomic Structure of Palladium Nanoparticles during the Desorption of Hydrogen According to X-Ray Diffraction

A. L. Bugaev[a], *, A. A. Guda[a], **, K. A. Lomachenko[b], and A. V. Soldatov[a]

[a] *International Smart Materials Research Institute, Southern Federal University, Rostov-on-Don, 344090 Russia*
[b] *European Synchrotron Radiation Facility, 38043 Grenoble Cedex 9, France*
**e-mail: arambugaev@gmail.com*
***e-mail: guda@sfedu.ru*

Received March 11, 2019; revised March 27, 2019; accepted March 27, 2019

The process of desorption of hydrogen from small palladium nanoparticles is recorded by time-resolved synchrotron X-ray diffraction. Changes in the diffraction profiles corresponding to the transition from the palladium β phase to the α phase are detected. The model of the continuous change in the size of the β-phase region can be excluded, since the full-profile analysis by the Rietveld method did not reveal broadening of the diffraction peaks corresponding to the palladium crystal lattice during desorption. The theoretical simulation shows the presence of a surface/core interface with different average cell parameters. However, the near-surface layers of the nanoparticle make a lower contribution to the observed diffraction reflections because of a worse crystallinity. The cell parameter in the nanoparticle core depends on the hydrogen concentration in the core itself and in the shell in view of the presence of stresses at the interface.

DOI: 10.1134/S002136401909008X

1. INTRODUCTION

The formation of the hydride phase of palladium is one of the most striking examples of a first-order phase transition in which there is an abrupt change in the volume of the sample upon the transition from the pure metallic to the α- hydride phase and from the α phase to the β phase of palladium hydride. For the fundamental understanding of such a phase transition, the Ising model is commonly used [1]. However, the thermodynamics and kinetics of the corresponding phase transitions in real systems become more complex in view of the effect of microstresses and other factors [2, 3].

Over the past decades, phase transitions in metal hydrides were actively studied both theoretically and experimentally [4, 5]. More recent studies were focused on nanomaterials [6–10] and revealed that the existence of individual α and β phases of palladium hydride are observed in nanoparticles, up to sizes of about 1.5 nm. It is obvious that the thermodynamics and kinetics of phase transitions in nanoparticles largely depend on their shape and size. At the same time, particular interest in studying the kinetics of adsorption and desorption of hydrogen is due to their use in the catalytic industry, where hydrogen is most reactive when accumulated in the form of β-hydride in the bulk of nanoparticles [11].

At the same time, reported experimental data of the kinetics of the atomic and electronic structure of palladium during phase transitions are currently scarce. First of all, this is because the processes of hydrogen adsorption and desorption occur in nanoparticles in several seconds [12]. Energy-dispersive X-ray spectroscopy showed that the process of hydrogen absorption by palladium nanoparticles at atmospheric pressure lasts for about 0.2 s [13]. Therefore, the characteristic times of phase transitions are expected at the same or smaller time scales and their detection is a difficult experimental task.

In this work, the kinetics of the atomic structure of palladium nanoparticles during hydrogen desorption at various temperatures is studied. The kinetics of the atomic and electronic structures is analyzed by powder X-ray diffraction using synchrotron radiation. The diffraction profiles are recorded by a two-dimensional detector, which makes it possible to achieve the optimal data quality in short measurement times.

2. METHODS

In this work, a sample of an industrial catalyst based on palladium nanoparticles on a carbon substrate was used [14]. Nanoparticles had the average diameter $D = 2.6$ nm and a narrow size distribution (standard deviation $\sigma = 0.4$ nm). We previously characterized the sample in detail by the methods of transmission electron microscopy, gas porosimetry, powder X-ray diffraction, and X-ray absorption spectros-

copy [10, 15–18]. X-ray diffraction patterns were measured at the BM01B beamline [19] of the European Synchrotron Radiation Facility (Grenoble, France). A Si (111) monochromator isolated a wavelength of 0.50544 Å from the radiation emitted from a dipole magnet. A CMOS-DEXELA 2D detector was located at a distance of 250.24 mm from the sample, which made it possible to record the angular range from 2° to 52° (d_{min} = 0.58 Å). The wavelength of the incident X-rays, the distance between the sample and the detector, and the slope of the detector were optimized by the Rietveld method for LaB_6 and Si samples and were fixed when specifying the structure of the Pd/C samples. For the best statistics, 20 diffraction images and 20 dark images (without the X-ray beam) with a recording time of 5 s were measured at each experimental point. Two-dimensional images were processed by the PyFAI software program [20], which performs fast averaging, background subtraction, and image integration for $I(2\theta)$ curves. A full-profile Rietveld analysis was performed using the Jana2006 code [21]. The initial profile parameters were specified by fitting the diffraction profiles for nanoparticles without hydrogen and with the maximum hydrogen concentration at each temperature. In the final fitting, we optimized the fractions of the α and β phases and the cell parameters corresponding to each phase.

X-ray diffraction during hydrogen desorption from palladium nanoparticles was measured with a time resolution of 3 scans per second in the temperature range from 273 to 293 K (0–20°C). Higher temperatures were not used, since the characteristic hydrogen desorption time for them was less than 1 s and the time resolution of the facility was not sufficient for the effective detection of this process. Lower temperatures were not used because of the formation of an ice shell on the capillary surface contributing to the diffraction data. Initially, the sample was in a pure hydrogen atmosphere at a pressure of 500 mbar. Then, hydrogen was evacuated in a time less than 0.3 s through an open fast pneumatic valve. For all studied temperatures, changes in the diffraction profiles were saturated in a time of about 10 s.

To calculate diffraction data, we considered four hydrogen distribution models: (i) a particle without hydrogen, (ii) a uniform $PdH_{0.5}$ distribution, (iii) hydrogen in the inner region (core) with the $PdH_{0.5}$ stoichiometry, and (iv) hydrogen in the near-surface layers (shell) with the $PdH_{0.5}$ stoichiometry. The diameter of the palladium nanoparticle was 3 nm, or 960 atoms. All models were optimized within the electron density functional theory using the VASP 5.2 software package [22, 23]. The size of the plane wave basis was determined by the parameter ENCUT = 240 eV; the first-order Methfessel–Paxton method with a smearing width of 0.2 eV (ISMEAR = 1, SIGMA = 0.2) was used to determine the population of orbitals. For relaxation of the structure, the quasi-Newtonian method was used (IBRION = 1); the whole particle was placed in a supercell with an edge length of 40 Å, which was fixed during the optimization (ISIF = 2). The convergence in energy within the self-consistency cycle was better than 0.1 meV. The geometry relaxation was considered complete when the energy between successive deformation cycles was less than 0.01 eV, which required 200 cycles of geometric iterations on average (about 30 days on a 6-core Intel Original Core i7 X6 5930 K processor @ 3.5 GHz (Haswell), 64 GB DDR4). After the optimization, the resulting models were used to calculate diffraction patterns by the Debye method [24].

3. RESULTS AND DISCUSSION

Examples of experimental diffraction patterns measured at 273 K are shown in Fig. 1 and make it possible to estimate the quality of data measured with an exposure of 0.3 s. The shape and positions of the peaks of the diffraction profiles correspond to the data obtained earlier for palladium nanoparticles under steady-state conditions [15–18, 25, 26], indicating that a gradual transition from the palladium hydride phase to a pure metallic state occurs during hydrogen desorption. The sample at the initial time and after 10 s is in pure single-phase states, whereas intermediate two-phase states can be observed on diffraction patterns measured in 2 and 4 s after hydrogen is pumped out of a capillary (Fig. 1).

The full-profile analysis of all diffraction patterns obtained was carried out for the quantitative analysis of the kinetics of the atomic structure of the palladium nanoparticles during hydrogen desorption. As a result, the cell parameters and relative concentrations of the α and β phases were determined. Figure 2 shows the

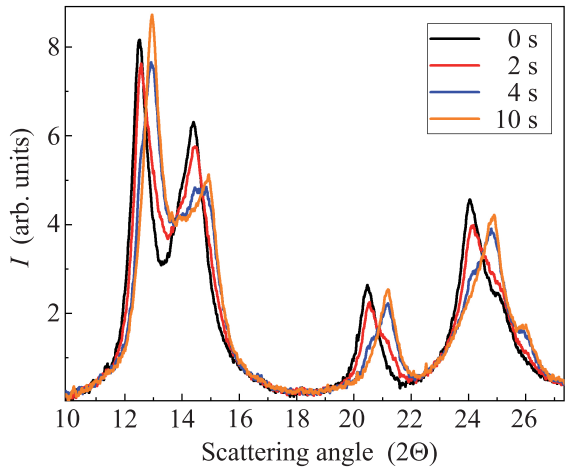

Fig. 1. (Color online) Diffraction profiles varying in the process of hydrogen desorption at a temperature of 273 K. The numbers indicate the time in seconds that elapsed after the opening of the pneumatic valve for the evacuation of hydrogen from the capillary.

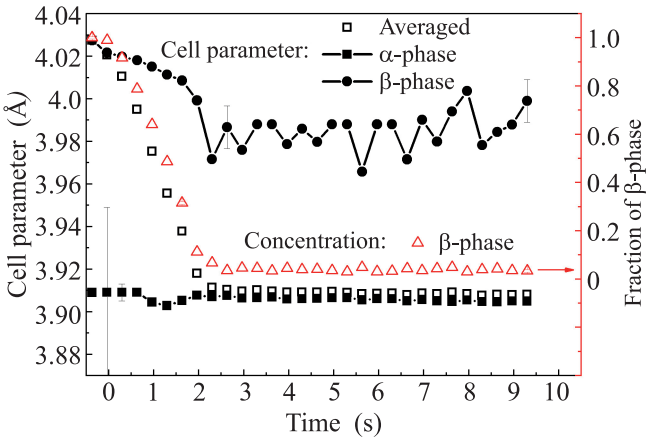

Fig. 2. (Color online) Results of the full-profile analysis of a series of diffraction patterns measured in the course of hydrogen desorption at a temperature of 273 K. The cell parameters determined for the (curve with squares) α phase, (curve with circles) β phase, and (black open squares) averaged cell parameters. Red triangles denote the fraction of the β phase (right axis of ordinates).

results of the full-profile analysis for a series of diffraction patterns measured at a temperature of 273 K, at which the phase transition kinetics is the slowest.

According to the data presented in Fig. 2, a phase transition occurs during hydrogen desorption from palladium nanoparticles similar to that observed in quasistatic measurements, where the hydrogen pressure gradually changes from pure vacuum to 1 atm [10, 15, 16, 18, 27]. At the same time, the coexistence of palladium α- and β-hydride phases is detected at certain times during the observed structural changes. The results of the full-profile analysis of diffraction data for various temperatures (Fig. 3) indicate the temperature dependence of the phase transition time. Figure 3a shows the change in the average cell parameter a calculated by the formula

$$a = (1 - n) \cdot a_\alpha + n \cdot a_\beta, \qquad (1)$$

where a_α and a_β are cell parameters in the α and β phases, respectively, and n is the fraction of the β phase.

The mechanism of hydrogen desorption from palladium hydride nanoparticles is also actively discussed in the literature. In particular, in a number of works [12, 28, 29], a model of the core–shell type is proposed, in which a hydrogen-depleted core and a hydride shell are formed during hydrogen desorption. However, the results of our full-profile analysis show that the profile parameters of the pseudo-Voigt function remain almost unchanged during the entire desorption process. A possible reason for this behavior should be the small size of nanoparticles, in which the coexistence of two phases within one particle would be difficult. Thus, the phase transition in the volume of

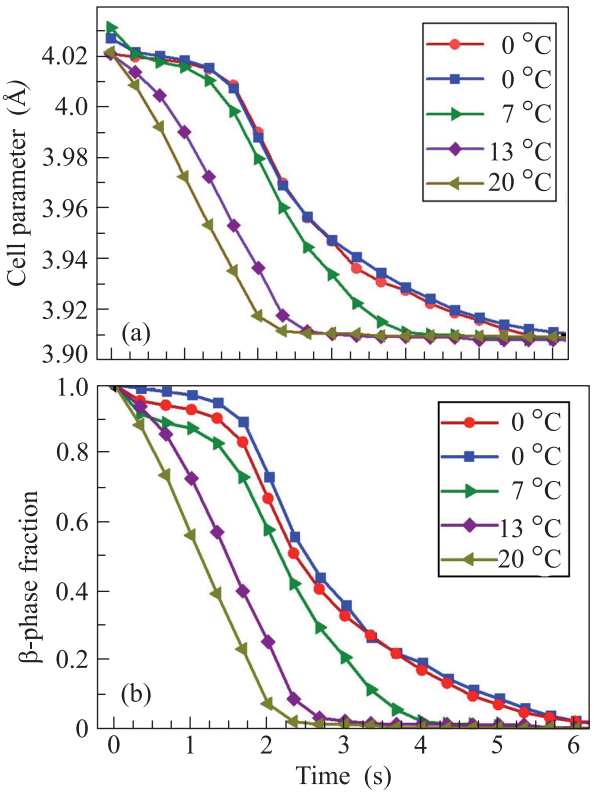

Fig. 3. (Color online) Kinetics of changes in the atomic structure of palladium nanoparticles determined from the X-ray diffraction data. (a) Change in the average cell parameter calculated by Eq. (1). (b) Change in the concentration of the β phase of palladium hydride in the sample.

each individual particle occurs abruptly, in much the same way as bulk palladium. Theoretical calculations below demonstrate that this statement is true only in part. Regions with different average interatomic distances can be distinguished even in a small nanoparticle because of a nonuniform hydrogen distribution. However, the stresses at the interface tend to equalize these values.

The changes in the cell parameter for different temperatures observed over diffraction have two stages. The first is the release of hydrogen from the surface of the nanoparticles. At the same time, in the inner region (core), the hydrogen concentration varies only slightly. As we show below, the observed diffraction data are mainly affected by the crystalline core, while changes in the shell of the nanoparticles contribute less. The first stage is longer for low temperatures (in the interval of 0–1.5 s for 0°C) than for high ones. The second stage is characterized by a sharp decrease in the cell parameter and the fraction of the β phase. For a temperature of 20°C, the second phase begins almost immediately after the start of the experiment. This process corresponds to the diffusion of hydrogen atoms in the near-surface layers and the subsequent

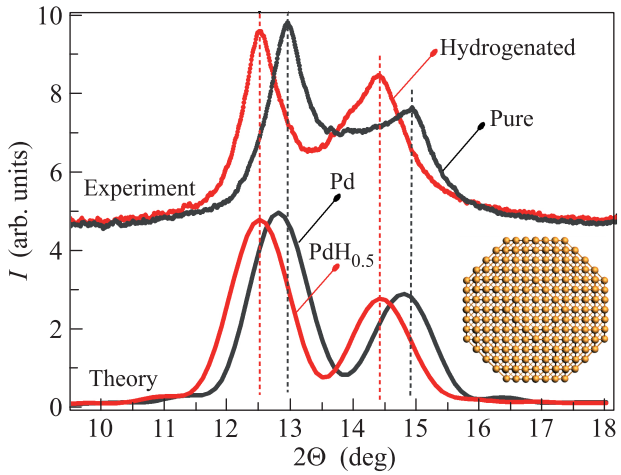

Fig. 4. (Color online) Experimental diffraction patterns for pure palladium and palladium hydride nanoparticles at a hydrogen pressure of 1 bar in comparison with those calculated for optimized structures with Pd and $PdH_{0.5}$ stoichiometries. The inset shows the nanoparticle model used to optimize the structure, as well as to calculate the diffraction patterns and the radial distribution function (see Fig. 5).

phase transition of the core to the α phase. The delay in the release of hydrogen atoms from the core is explained by the presence of stresses in the lattice at the interface between the inner region of the nanoparticles and the outer surface layers. A slower diffusion compared to the dissociation of hydrogen molecules was previously observed in experiments with palladium membranes [30]. We confirm below the presence of internal stresses in small palladium nanoparticles using the ab initio simulation.

Figure 4 shows the experimental and theoretical diffraction patterns for pure palladium nanoparticles and those with the maximum hydrogen concentration. The reflections on the theoretical diffraction pattern for Pd nanoparticles are slightly shifted toward lower angles with respect to the experimental data by approximately 0.15°, which is due to an error of 1–2% in the cell parameters determined by the electron density functional method and to the effects of the size of the basis set. When hydrogen is included in the palladium structure, the interatomic distances increase and the diffraction maxima shift toward smaller angles, which is reproduced well by theoretical calculations.

Changes in the structure of nanoparticles with different hydrogen distributions were analyzed using the radial distribution function (RDF). The RDF was calculated for each atom in optimized structures. Then, the RDF was averaged for the inner region with a diameter of 2.4 nm (hereinafter referred to as the core) and for the outer region containing approximately two near-surface layers (hereinafter, the shell). A diameter of 2.4 nm for the separation into the core and the shell was chosen because this region contains about half of the total number of the palladium atoms in a nanoparticle with a diameter of 3 nm. Figure 5a shows the averaged pairs of RDFs for four models of nanoparticles with hydrogen. The data obtained carry important information about the distribution of the α and β phases of palladium in the nanoparticle. The common result for all models is the reduced Pd–Pd distances in the shell compared to the core. In addition, the width of the RDF in the shell for all models is much larger than that in the core, which indicates the structural disorder because of the relaxation of near-surface atoms.

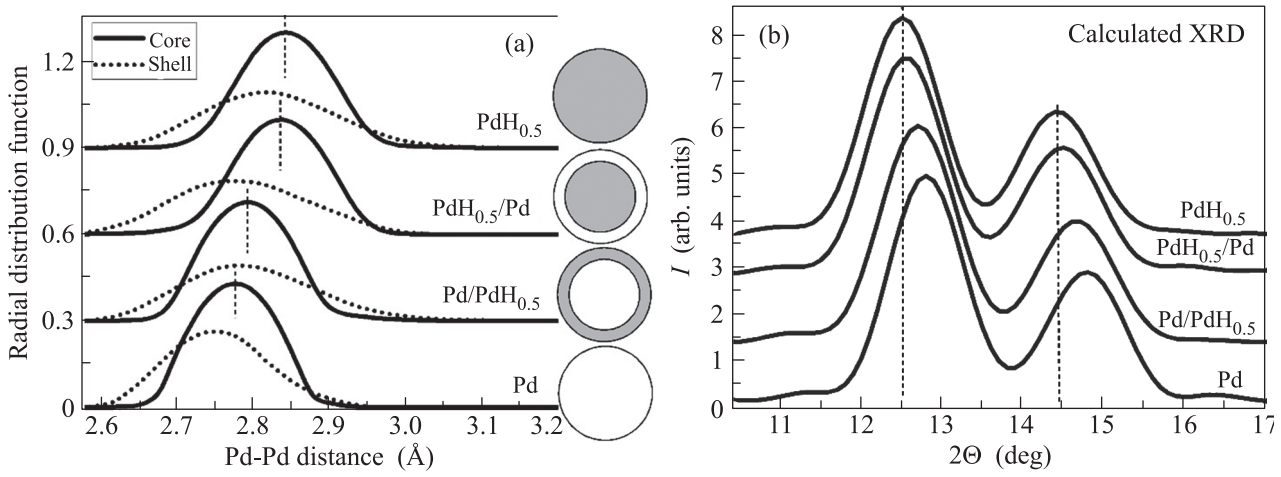

Fig. 5. (a) Calculated radial distribution functions for structures of optimized palladium nanoparticles with a diameter of 3 nm. Solid and dotted lines are averaged radial distributions for the inner region of a nanoparticle with a diameter of 2.4 nm and for near-surface layers, respectively. Detailed description of hydrogen distribution models is given in the main text. (b) Calculated Debye diffraction patterns for models of nanoparticles shown in panel (a).

At the release of all hydrogen atoms from the shell (the transition from $PdH_{0.5}$ to $PdH_{0.5}$/Pd), the average interatomic distance in the shell changes by 0.05 Å. At the same time, the Pd–Pd distance inside the core also changes in view of the arising stresses at the interface. This change is about 0.01 Å. Then, with the hydrogen redistribution from the core to the shell (the transition from $PdH_{0.5}$/Pd to Pd/$PdH_{0.5}$), the Pd–Pd distance in the core decreases to 2.79 Å, which is approximately 0.02 Å larger than that in the core of a pure Pd nanoparticle. Finally, the Pd–Pd distances in the pure palladium nanoparticle decrease to 2.77 Å in the core and to 2.75 Å in the shell.

Figure 5b shows the calculated diffraction patterns for the models under discussion. Despite successive phase transitions in the shell and core, the diffraction profiles have a very close width, and their shifts correspond mainly to the changes in the Pd–Pd distances in the core of the nanoparticles. The smaller effect of the shell on the diffraction data can be explained by the worse crystallinity of the shell because of surface relaxation. Thus, the main contribution to the experimental diffraction data comes from the crystal core. In this case, the cell parameter in the core depends to a large extent on the hydrogen content in the core and to a lesser extent on the presence of hydrogen in the shell. The effect of interatomic distances in the shell on the cell parameter in the core of a small nanoparticle is explained by the large relative area of the interface between the two phases and the stresses at the interface.

4. CONCLUSIONS

In this work, hydrogen desorption from nanoparticles palladium with a diameter of about 3 nm has been studied. The cell parameter and the ratio between the α and β phases of palladium have been determined from the full-profile analysis of diffraction patterns measured with a time resolution better than 0.3 s for temperatures of 0–20°C. At low temperatures, two stages have been found in the kinetics of the decrease in the cell parameter. In the first stage, hydrogen escapes from the near-surface layers of the nanoparticle, which leads to small changes in the average cell parameter of the nanoparticles. In the second stage, hydrogen is released from the core with the phase transition of the core from the α phase to the β phase. Using the geometric optimization of nanoparticles with different hydrogen distribution inside, the presence of two regions in the nanoparticle—the shell and the core—has been established. In this case, the Pd–Pd in-shell distances are always smaller than the in-core distance, which leads to the presence of a potential barrier for hydrogen to escape from the core and confirms the time delay of the phase transition observed in the experiment. Because of the violation of the crystallinity of the shell, which is noticeable in the broadening of the radial distribution function of atoms, the main contribution to diffraction reflections comes only from the core of nanoparticles.

This work was supported by the Russian Science Foundation (project no. 17-72-10245).

REFERENCES

1. K. Binder, Phys. Rev. Lett. **45**, 811 (1980).
2. E. A. Brener, V. I. Marchenko, and R. Spatschek, Phys. Rev. E **75**, 041604 (2007).
3. R. B. Schwarz and A. G. Khachaturyan, Phys. Rev. Lett. **74**, 2523 (1995).
4. A. Borgschulte, R. Gremaud, and R. Griessen, Phys. Rev. B **78**, 094106 (2008).
5. V. P. Zhdanov, A. Krozer, and B. Kasemo, Phys. Rev. B **47**, 11044 (1993).
6. M. Yamauchi, R. Ikeda, H. Kitagawa, and M. Takata, J. Phys. Chem. C **112**, 3294 (2008).
7. H. Jobic and A. Renouprez, J. Less-Common Met. **129**, 311 (1987).
8. B. Ingham, M. F. Toney, S. C. Hendy, T. Cox, D. D. Fong, J. A. Eastman, P. H. Fuoss, K. J. Stevens, A. Lassesson, and S. Brown, Phys. Rev. B **78**, 245408 (2008).
9. D. Narehood, S. Kishore, H. Goto, J. Adair, J. Nelson, H. Gutierrez, and P. Eklund, Int. J. Hydrogen Energ. **34**, 952 (2009).
10. A. L. Bugaev, A. A. Guda, K. A. Lomachenko, L. A. Bugaev, and A. V. Soldatov, Bull. Russ. Acad. Sci.: Phys. **79**, 1180 (2015).
11. D. Teschner, J. Borsodi, A. Wootsch, Z. Revay, M. Havecker, A. Knop-Gericke, S. D. Jackson, and R. Schlögl, Science (Washington, DC, U. S.) **320**, 86 (2008).
12. C. Langhammer, V. P. Zhdanov, I. Zoric, and B. Kasemo, Phys. Rev. Lett. **104**, 135502 (2010).
13. D. Matsumura, Y. Okajima, Y. Nishihata, and J. Mizuki, J. Alloys Compd. **509**, S849 (2011).
14. A. Piovano, A. Lazzarini, R. Pellegrini, G. Leofanti, G. Agostini, S. Rudić, A. L. Bugaev, C. Lamberti, and E. Groppo, Adv. Condens. Matter Phys. **2015**, 803267 (2015).
15. A. L. Bugaev, A. A. Guda, K. A. Lomachenko, V. V. Shapovalov, A. Lazzarini, J. G. Vitillo, L. A. Bugaev, E. Groppo, R. Pellegrini, A. V. Soldatov, J. A. van Bokhoven, and C. Lamberti, J. Phys. Chem. C **121**, 18202 (2017).
16. A. L. Bugaev, A. A. Guda, K. A. Lomachenko, A. Lazzarini, V. V. Srabionyan, J. G. Vitillo, A. Piovano, E. Groppo, L. A. Bugaev, A. V. Soldatov, V. P. Dmitriev, R. Pellegrini, J. A. van Bokhoven, and C. Lamberti, J. Phys.: Conf. Ser. **712**, 012032 (2016).
17. A. L. Bugaev, A. A. Guda, A. Lazzarini, K. A. Lomachenko, E. Groppo, R. Pellegrini, A. Piovano, H. Emerich, A. V. Soldatov, L. A. Bugaev, V. P. Dmitriev, J. A. van Bokhoven, and C. Lamberti, Catal. Today **283**, 119 (2017).
18. A. L. Bugaev, O. A. Usoltsev, A. Lazzarini, K. A. Lomachenko, A. A. Guda, R. Pellegrini, M. Carosso, J. G. Vitillo, E. Groppo, J. A. van Bokhoven, A. V. Soldatov, and C. Lamberti, Faraday Discuss. **208**, 187 (2018).

19. W. van Beek, O. V. Safonova, G. Wiker, and H. Emerich, Phase Trans. **84**, 726 (2011).
20. J. Kieffer and J. P. Wright, Powder Diffract. **28**, S339 (2013).
21. V. Petříček, M. Dušek, and L. Palatinus, Zeitschr. Kristallogr. – Cryst. Mater. **229**, 345 (2014).
22. P. E. Blochl, Phys. Rev. B **50**, 17953 (1994).
23. G. Kresse and J. Furthmüller, Phys. Rev. B **54**, 11169 (1996).
24. N. Pinna, in *Scattering Methods and the Properties of Polymer Materials,* Ed. by N. Stribeck and B. Smarsly (Springer, Berlin, Heidelberg, 2005), p. 29.
25. A. A. Skorynina, A. A. Tereshchenko, O. A. Usoltsev, A. L. Bugaev, K. A. Lomachenko, A. A. Guda, E. Groppo, R. Pellegrini, C. Lamberti, and A. Soldatov, Radiat. Phys. Chem. (in press). https://doi.org/10.1016/j.radphyschem.2018.11.033
26. A. L. Bugaev, A. A. Guda, I. A. Pankin, E. Groppo, R. Pellegrini, A. Longo, A. V. Soldatov, and C. Lamberti, Catal. Today **24**, 103954 (2019).
27. A. L. Bugaev, A. A. Guda, K. A. Lomachenko, V. V. Srabionyan, L. A. Bugaev, A. V. Soldatov, C. Lamberti, V. P. Dmitriev, and J. A. van Bokhoven, J. Phys. Chem. C **118**, 10416 (2014).
28. C. Wadell, T. Pingel, E. Olsson, I. Zoric, V. P. Zhdanov, and C. Langhammer, Chem. Phys. Lett. **603**, 75 (2014).
29. V. P. Zhdanov and B. Kasemo, Chem. Phys. Lett. **460**, 158 (2008).
30. B. D. Kay, C. H. F. Peden, and D. W. Goodman, Phys. Rev. B **34**, 817 (1986).

Translated by L. Mosina

SPELL: OK